Renal Mass Imaging with MRI Clear Cell Likelihood Score: A User's Guide

Anup S. Shetty, MD • Tyler J. Fraum, MD • David H. Ballard, MD • Mark J. Hoegger, MD, PhD • Malak Itani, MD • Mohamed Z. Rajput, MD
Michael H. Lanier, MD • Brian M. Cusworth, MD • Amanda L. Mehrsheikh, MD • Jorge A. Cabrera-Lebron, MD • Jia Chu, MD
Christopher R. Cunningham, MD • Ryan S. Hirschi, MD • Mahati Mokkarala, MD • Jackson G. Unteriner, MD • Eric H. Kim, MD
Cary L. Siegel, MD • Daniel R. Ludwig, MD

Author affiliations, funding, and conflicts of interest are listed at the end of this article.
See the invited commentary by Pedrosa in this issue.

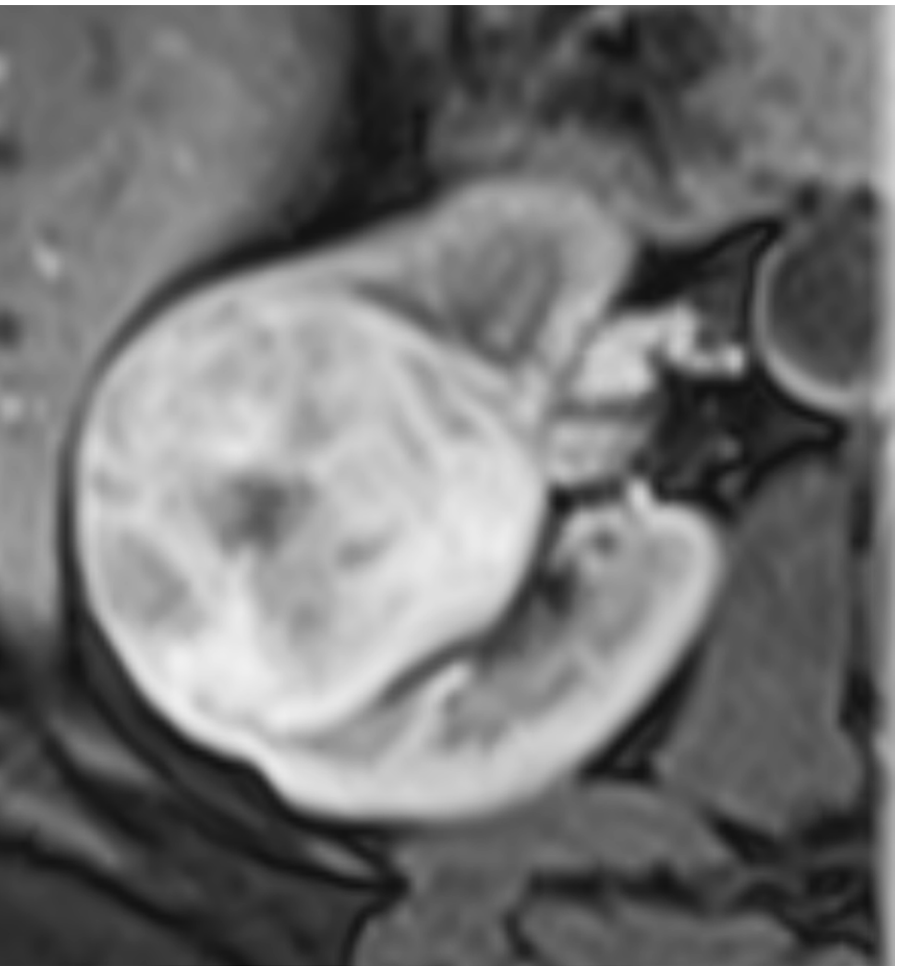

Small solid renal masses (SRMs) are frequently detected at imaging. Nearly 20% are benign, making careful evaluation with MRI an important consideration before deciding on management. Clear cell renal cell carcinoma (ccRCC) is the most common renal cell carcinoma subtype with potentially aggressive behavior. Thus, confident identification of ccRCC imaging features is a critical task for the radiologist. Imaging features distinguishing ccRCC from other benign and malignant renal masses are based on major features (T2 signal intensity, corticomedullary phase enhancement, and the presence of microscopic fat) and ancillary features (segmental enhancement inversion, arterial-to-delayed enhancement ratio, and diffusion restriction). The clear cell likelihood score (ccLS) system was recently devised to provide a standardized framework for categorizing SRMs, offering a Likert score of the likelihood of ccRCC ranging from 1 (very unlikely) to 5 (very likely). Alternative diagnoses based on imaging appearance are also suggested by the algorithm. Furthermore, the ccLS system aims to stratify which patients may or may not benefit from biopsy. The authors use case examples to guide the reader through the evaluation of major and ancillary MRI features of the ccLS algorithm for assigning a likelihood score to an SRM. The authors also discuss patient selection, imaging parameters, pitfalls, and areas for future development. The goal is for radiologists to be better equipped to guide management and improve shared decision making between the patient and treating physician.

Introduction

Small solid renal masses (SRMs), defined as solid (>25% of the lesion exhibiting enhancement) renal masses less than 4 cm in diameter, are a frequent incidental cross-sectional imaging finding (1). Eighty percent of SRMs are malignant, with clear cell renal cell carcinoma (ccRCC) being the most common subtype of renal cell carcinoma (RCC) (2). Some subtypes of RCC, such as papillary RCC (pRCC) or chromophobe RCC (chrRCC), often exhibit indolent behavior (as do some low-grade ccRCCs) and may be safely surveilled for growth rather than definitively managed with resection or ablation. The clear cell likelihood score (ccLS) system was devised in recent years to create a systematic approach for assessing the MRI features of SRMs and assigning a ccRCC likelihood score (3–6). Comprehensive SRM assessment includes integrating many contributing imaging features, which can make interpretation challenging. Stating that an enhancing SRM is suspicious for RCC does not adequately advance the care of the patient. The ccLS system guides both novice and experienced abdominal imagers and allows organized SRM assessment,

Supplemental Material

RadioGraphics 2023; 43(7):e220209
https://doi.org/10.1148/rg.220209

Content Codes: GU, MR

CME Quiz questions for this article are available in the supplemental material.

Invited Commentary

Abbreviations: ADC = apparent diffusion coefficient, ADER = arterial-to-delayed enhancement ratio, AML = angiomyolipoma, ccRCC = clear cell RCC, ccLS = clear cell likelihood score, chrRCC = chromophobe RCC, CMP = corticomedullary phase, DFP = disease-focused panel, DWI = diffusion-weighted imaging, fpAML = fat-poor angiomyolipoma, pRCC = papillary RCC, RCC = renal cell carcinoma, SEI = segmental enhancement inversion, SRM = solid renal mass

TEACHING POINTS

- The ccLS algorithm should be applied only to solid masses (>25% solid enhancing component) without macroscopic fat.
- Renal protocol MRI should meet minimum technical standards, as recommended by the Society of Abdominal Radiology Disease-Focused Panel on Renal Cell Carcinoma, when applying the ccLS algorithm.
- With the ccLS algorithm, the clinician is provided a Likert score reflecting the likelihood of ccRCC. The score choices include 1 (very unlikely), 2 (unlikely), 3 (intermediate likelihood), 4 (likely), and 5 (very likely).
- After a ccLS is determined, the algorithm also offers other entities to consider in the differential diagnosis on the basis of the combination of imaging features present, such as oncocytoma with SEI, fpAML with an ADER equal to or greater than 1.5 and marked diffusion restriction, pRCC with T2-weighted hypointensity and mild CMP enhancement, and chRCC based on variable T2-weighted and CMP characteristics.
- Subtraction imaging is not formally used in the ccLS scheme in assessing the pattern of CMP enhancement but provides a simpler method of assessing the intensity of enhancement, as precontrast T1-weighted signal intensity is automatically factored into the subtracted sequence signal intensities of the SRM and renal cortex.

thus providing more complete renal lesion characterization. The ccLS characterization can influence management, such as obviating biopsy of SRMs with a low or high ccLS and appropriately suggesting biopsy for SRMs with an intermediate ccLS.

In this article, we provide a guide for using the ccLS system to assess an SRM by outlining imaging parameters and protocol design; discuss when to apply the ccLS algorithm; and describe the algorithm's application, pitfalls, and areas for future development. A series of case examples depict the steps and nuances in using the ccLS system. The reader should feel equipped to use the ccLS system in assessing an SRM to provide optimal value to the patient and urologist.

Background

Renal masses, a common incidental finding, are increasingly recognized owing to the expanding role of cross-sectional imaging (7). Many incidental SRMs cannot be characterized at the time of detection because of indeterminate imaging features on a noncontrast or single-phase contrast-enhanced CT examination (8). In such cases, a dedicated renal examination is required to determine whether a mass represents a benign cyst or solid renal neoplasm (9). Among SRMs further characterized as solid and enhancing, up to 20% represent benign lesions such as angiomyolipoma (AML) or oncocytoma, with an even higher frequency of benignity among lesions less than 1 cm in size (3,10). Furthermore, although the majority of SRMs represent RCCs, many exhibit indolent behavior and rarely metastasize when small (ie, SRM <4 cm) (11,12).

Accordingly, the increasing detection of RCC and higher rates of surgical therapy have not resulted in a decrease in mortality for RCC (13). Therefore, radiologists and urologists are frequently presented with management challenges when encountering SRMs because they are common, often benign, and, if malignant, frequently indolent. Improvements in risk stratification would help identify patients who can safely enroll in active surveillance rather than undergo invasive procedures such as biopsy, ablation, or resection. This would be especially helpful among patients who are older and/or have comorbidities; active surveillance carries a low risk of development of metastatic disease (<2%) and has a comparable mortality rate to that of definitive therapy in appropriately selected patients (14).

Among commonly encountered RCC subtypes, the clear cell subtype (ie, ccRCC) is typically most aggressive (15). Confirmation of malignant histologic findings and subtyping of RCC can be accomplished with percutaneous biopsy. However, biopsy has its own set of considerations and risks. First, biopsy may not be feasible in all cases, such as in a patient with coagulopathy or certain tumor locations without a safe percutaneous window. Second, biopsy is invasive and has substantial potential risks (albeit low rates of complications) including life-threatening hemorrhage (16). Finally, the biopsy may be nondiagnostic in up to 20% of cases owing to sampling error, insufficient tissue, and/or a cystic change or necrosis within the tumor (17). In our practice, renal biopsy is used only in selected cases, such as for borderline surgical candidates, patients with current or prior nonrenal malignancy (eg, lymphoma or melanoma), surgical planning in the setting of multifocal disease, and concurrent percutaneous ablation. An expanding body of literature has identified imaging features that help radiologists predict the histopathologic characteristics of an SRM, potentially obviating biopsy for treatment decisions (5). This so-called virtual biopsy can be performed concomitantly with dedicated renal protocol MRI, without an added risk or cost to the patient.

An important limitation of imaging in renal lesion characterization is a lack of adequate standardization, leading to subjectivity of interpretation. To address this limitation, the ccLS system, a standardized framework for categorizing SRMs, was initially developed at the University of Texas Southwestern Medical Center in 2017 (version 1.0) and later revised in 2022 (version 2.0) (6,18). The ccLS algorithm is based on multiparametric MRI rather than CT owing to its ability to help detect microscopic (intravoxel) fat, characterize tumor cellularity by using diffusion-weighted imaging (DWI), and acquire multiple dynamic postcontrast phases without ionizing radiation. The ccLS system is used to categorize SRMs on the basis of the probability that an SRM represents ccRCC according to a Likert scale from 1 through 5, where 1 is very unlikely and 5 is very likely. In multicenter internal and external validation studies, a ccLS of 4 or more had a moderate to high sensitivity (75%–85%) and specificity (78%–82%) for the diagnosis of ccRCC, with moderate to near-perfect interobserver agreement (κ, 0.58–0.82) (19,20). Importantly, a ccLS of 2 or

less had a high negative predictive value (88%) for ruling out ccRCC histology (19).

In a cohort of renal masses of any size, the percentage of ccRCC among each ccLS was 5% (ccLS 1), 6% (ccLS 2), 35% (ccLS 3), 78% (ccLS 4), and 93% (ccLS 5) (21). In a separate multicenter study of cT1a masses only (ie, ≤4 cm), the percentage of ccRCC among each ccLS was 6% (ccLS 1), 38% (ccLS 2), 33% (ccLS 3), 72% (ccLS 4), and 81% (ccLS 5) (19). A higher ccLS is also correlated with faster growth of an SRM (22). Taken together, these validation studies strongly support the role of the ccLS system in the risk stratification of SRMs in selected patients.

Patient Selection

The ccLS algorithm may be most valuable for assessing renal masses equal to or smaller than 4 cm (T1a designation in the American Joint Committee on Cancer TNM staging system), since a significant proportion of these masses will be benign or exhibit indolent behavior at follow-up. Although, in principle, the same radiologic algorithm would apply to SRMs larger than 4 cm (T1b or T2) and can be used for characterization, resection is typically advocated in that scenario (23). Nevertheless, assigning a ccLS may still be helpful if surveillance would be considered, such as in patients with significant comorbidities.

The ccLS algorithm should be applied only to solid masses (>25% solid enhancing component) without macroscopic fat. Cystic renal masses, defined as having less than 25% solid enhancing component, should be characterized by using the Bosniak classification system, which was most recently updated in 2019 (Fig 1) (24,25). The simple renal cysts and cystic components of renal masses can be identified by the homogeneous T2-weighted hyperintensity mirroring simple fluid elsewhere in the abdomen, such as cerebrospinal fluid or normal bile, and by the absence of enhancement or diffusion restriction (Fig 2) (26).

By comparison, hemorrhagic or proteinaceous cysts require careful assessment for enhancement with postcontrast T1-weighted sequences to arrive at the correct diagnosis, as they often exhibit confounding imaging features such as T2-weighted hypointensity, T1-weighted hyperintensity, and occasionally diffusion restriction. Subtraction sequences are of particular value for hemorrhagic or proteinaceous cysts, as the lesion should appear as a black hole on postcontrast images after the intrinsic T1-weighted hyperintensity is removed (Fig 3). Additional imaging features that can be helpful to identify hemorrhage include the presence of a rim of magnetic susceptibility from hemosiderin deposition, evidenced by in-phase signal intensity loss relative to that on the corresponding opposed-phase image, although this finding can also be seen with hemorrhagic RCCs.

Macroscopic fat is considered diagnostic of a classic (fat-rich) AML in the ccLS algorithm and obviates further characterization, with the caveat that RCC with osseous metaplasia (rare) could conceivably contain foci of macroscopic fat (27). Macroscopic fat can be diagnosed in several ways (Fig 4). The first method compares the signal intensity of an SRM on a T1- or T2-weighted image with and without the application of fat suppression, which can be performed with any method (frequency-selective fat saturation, inversion recovery, or the Dixon method) (28). Sequence parameters such as echo time and repetition time should ideally be as similar as possible between the standard and fat-suppressed sequences if this method is used to minimize effects upon signal weighting. The second method involves the use of chemical shift imaging to help assess the presence of an India ink artifact (type 2 chemical shift artifact) on opposed-phase images at the junction of the mass and normal renal parenchyma, indicating a fat-water interface. This may present challenges for exophytic masses at the poles of the kidney, where no normal kidney is in the imaging plane to identify the India ink artifact.

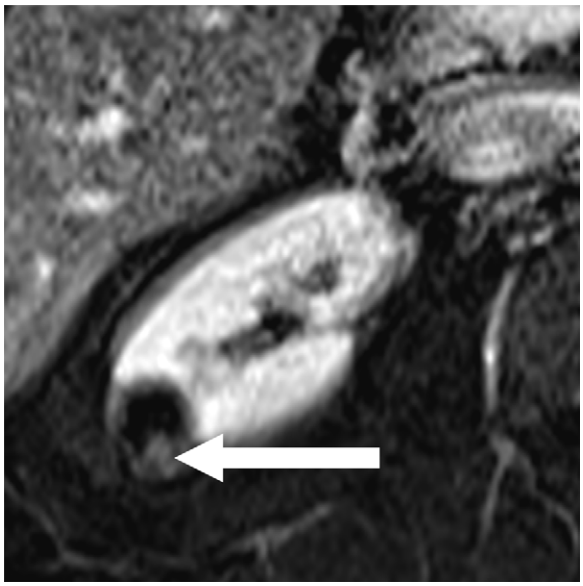

Figure 1. Cystic ccRCC in a 65-year-old man. Coronal postcontrast delayed phase T1-weighted MR image shows a cystic right lower pole renal mass best characterized by using the Bosniak classification system (version 2019) for cystic renal masses, with a Bosniak IV category determined on the basis of the presence of an enhancing nodule (convex protrusion with acute margins) larger than or equal to 4 mm (arrow). The ccLS should not be applied to cystic renal masses, defined as having less than 25% solid enhancing component. Grade 1 ccRCC was found at partial nephrectomy.

The third method is to compare the signal intensity of an SRM to that of adjacent retroperitoneal fat with a fat-only Dixon sequence, which is reconstructed from a chemical shift gradient-echo acquisition. Classic (fat-rich) AML should exhibit at least some foci of signal intensity similar to that of retroperitoneal fat, indicating the presence of macroscopic fat. Rarely, a large amount of iron or hemosiderin could result in hyperintense signal on fat-only Dixon images owing to aliasing. Thus, the signal intensity of macroscopic fat should be hyperintense on both fat-only Dixon and in-phase images. In practice, we use all three of these techniques for a comprehensive evaluation.

Imaging Protocol

Renal protocol MRI should meet minimum technical standards, as recommended by the Society of Abdominal Radiology Disease-Focused Panel (DFP) on Renal Cell Carcinoma, when applying the ccLS algorithm (29). Our imaging protocol at 1.5 T is detailed in the Table. In addition to sequences

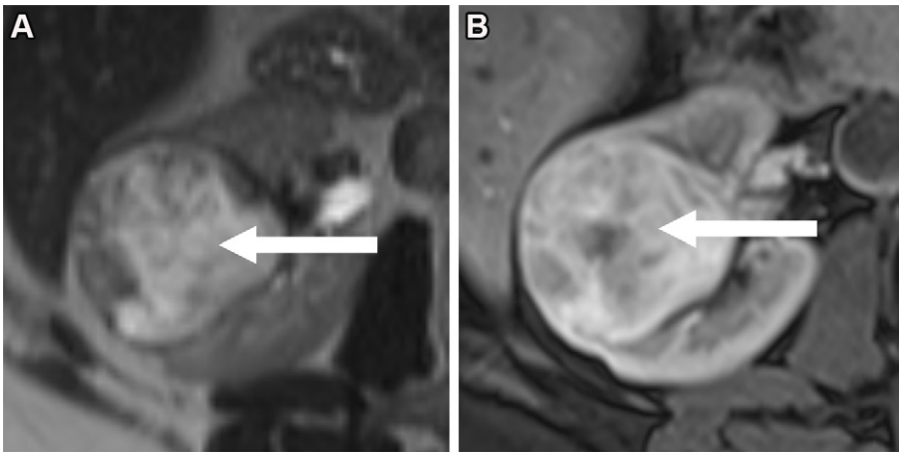

Figure 2. Probable ccRCC incidentally identified at MRI of the lumbar spine in a 39-year-old woman. **(A)** Axial T2-weighted MR image shows a heterogeneously T2-hyperintense mass (arrow), which might be mistakenly characterized as cystic at initial inspection. **(B)** Axial postcontrast corticomedullary phase (CMP) T1-weighted MR image shows solid enhancement (arrow). Microscopic fat was also present (not shown), with a ccLS of 5 (very likely ccRCC). An SRM should be characterized as cystic only after careful inspection at postcontrast imaging.

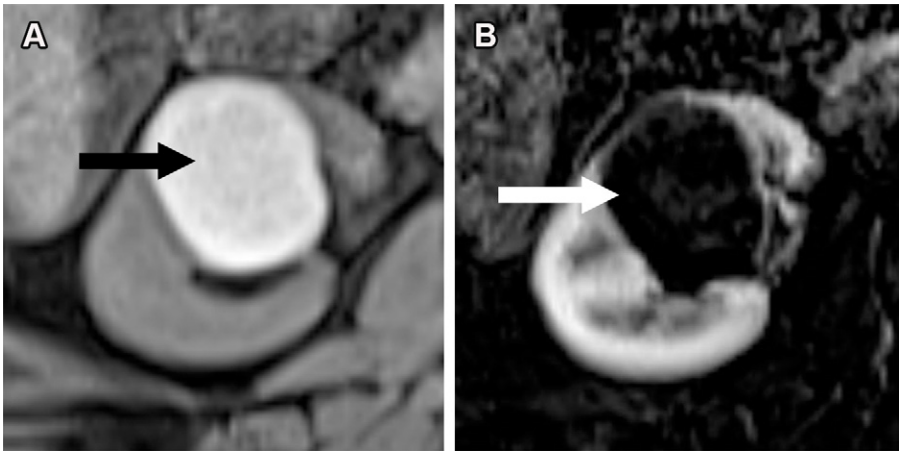

Figure 3. Hemorrhagic renal cyst in a 45-year-old woman with metastatic adenocarcinoma from an unknown primary site. **(A)** Axial precontrast T1-weighted MR image shows uniform T1 hyperintensity in a right renal mass (arrow). **(B)** Axial postcontrast CMP T1-weighted subtraction MR image shows no internal enhancement of the mass (arrow), consistent with a hemorrhagic cyst. Subtraction imaging is particularly helpful in assessing renal masses that exhibit intrinsic T1 hyperintensity to facilitate detection or exclusion of enhancement. The ccLS is not applied to hemorrhagic renal cysts.

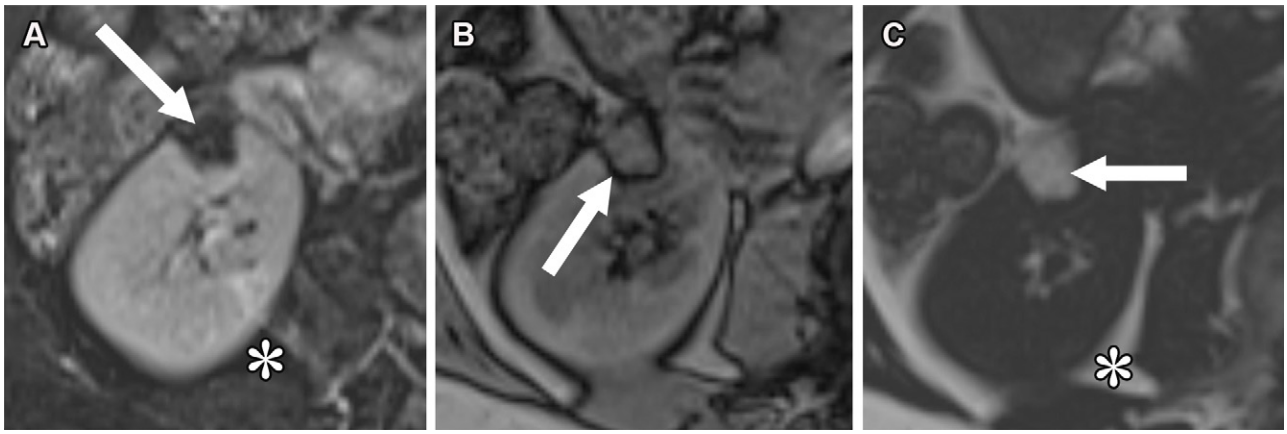

Figure 4. Classic (fat-rich) AML in a 45-year-old woman. **(A)** Axial fat-suppressed T2-weighted MR image shows hypointensity of a right renal mass (arrow) that is similar to that of retroperitoneal fat (*). The comparison T2-weighted MR image without fat suppression (not shown) showed a renal mass with similar signal intensity to that of fat. **(B)** Axial opposed-phase MR image shows an India ink artifact at the margin between the mass and normal kidney (arrow), indicating a fat-water interface. **(C)** Axial fat-only Dixon T1-weighted MR image shows hyperintensity of the mass (arrow), which matches that of retroperitoneal fat (*). All three of these findings can be used to diagnose a classic (fat-rich) AML, to which a ccLS should not be applied.

suggested by the Society of Abdominal Radiology DFP on RCC, our protocol includes T2-weighted multishot fast spin-echo sequences with and without fat suppression to detect macroscopic fat within an SRM by loss of signal intensity, an approach that may be more familiar to some readers. Macroscopic fat detection can also be accomplished by using the Dixon technique for chemical shift imaging, in which fat-only and water-only Dixon sequences are reconstructed from acquired opposed-phase and in-phase data. If a three-dimensional chemical shift sequence is used (as we do in our protocol) rather than the two-dimensional acquisition mentioned in the Society of Abdominal Radiology DFP on RCC protocol

Sample Protocol for Renal MRI

Sequence Name	Section Thickness (mm)	Matrix (pixels)	TR (msec)	TE (msec)	NSA	Acquisition Time (sec)	Notes
Coronal T2W single-shot fast SE	6	320 × 320	1000	100	1	90 (multiple breath holds)	Whole-abdomen coverage
Axial 3D Dixon T1W spoiled GRE	3	260 × 320	6.68	2.39, 4.77	1	14 (single breath hold)	Acquire in-phase and opposed-phase images, reconstruct fat-only and water-only images
Axial T2W single-shot fast SE	4	320 × 320	1000	100	1	120 (multiple breath holds)	Whole-abdomen coverage
Axial T2W fast SE	6	260 × 320	3000	93	1	40 (multiple breath holds)	Cover kidneys only; not part of DFP recommendations, optional sequence
Axial T2W fat-suppressed fast SE	6	260 × 320	3000	93	1	60 (multiple breath holds)	Cover kidneys only; not part of DFP recommendations, optional sequence
Axial single-shot DWI	6	256 × 268	9500	56	2, 4, 10	180 (free breathing)	Obtain *b* values of 50, 400, and 800 sec/mm^2; reconstruct ADC map
Axial 3D precontrast T1W spoiled GRE	3	260 × 320	5.09	2.33	1	12 (single breath hold)	...
Coronal 3D precontrast T1W spoiled GRE	3	260 × 320	5.09	2.33	1	12 (single breath hold)	...
Axial 3D T1W CMP spoiled GRE	3	260 × 320	5.09	2.33	1	12 (single breath hold)	30-sec delay or late arterial phase by bolus tracking or test bolus methods; generate subtraction images from precontrast acquisition
Axial 3D T1W venous phase spoiled GRE	3	260 × 320	5.09	2.33	1	12 sec (single breath hold)	70-sec delay; generate subtraction images from precontrast acquisition
Axial 3D T1W nephrographic phase spoiled GRE	3	260 × 320	5.09	2.33	1	12 sec (single breath hold)	150-sec delay; generate subtraction images from precontrast acquisition
Coronal 3D T1W delayed phase spoiled GRE	3	320 × 320	4.67	2.39	1	14 sec (single breath hold)	210-sec delay; generate subtraction images from precontrast acquisition
Axial 3D T1W delayed phase spoiled GRE	3	320 × 320	4.67	2.39	1	14 sec (single breath hold)	300-sec delay; generate subtraction from precontrast acquisition

Note.—CMP = corticomedullary phase, DFP = Society of Abdominal Radiology Disease-Focused Panel on Renal Cell Carcinoma, GRE = gradient-recalled echo, NSA = number of signal averages, SE = spin echo, TE = echo time, TR = repetition time, 3D = three dimensional, T1W = T1-weighted, T2W = T2-weighted.

and advocated by previous authors (6,30), adjusting the flip angle from the vendor default of 10° to 18° may improve detection and depiction of microscopic fat.

Imaging Parameters

The various imaging features used in the ccLS algorithm are summarized in Figure 5 (6). Details and nuances regarding each of the major and ancillary features are discussed in the following sections.

Major Features

T2-weighted Signal Intensity.—T2-weighted signal intensity is the first major feature of SRM assessment in the ccLS algorithm, with lesions considered as T2 hyperintense, isointense, or hypointense. T2-weighted characteristics of the SRM should be compared with those of the normal renal cortex on the same section with a non–fat-suppressed single-shot fast spin-echo T2-weighted sequence in the axial or coronal plane. We perform this sequence with thinner sections in the axial plane to avoid volume averaging, but a coronal acquisition is also helpful for facilitating cortical comparison for polar masses. The dominant signal intensity of the solid enhancing component of the mass should be assessed, as the nonenhancing component of a mass can vary in signal intensity depending on the presence of cystic change, necrosis, or hemorrhage. Often, the delayed phase postcontrast images can be useful when selecting a region of the mass for assessment of T2-weighted

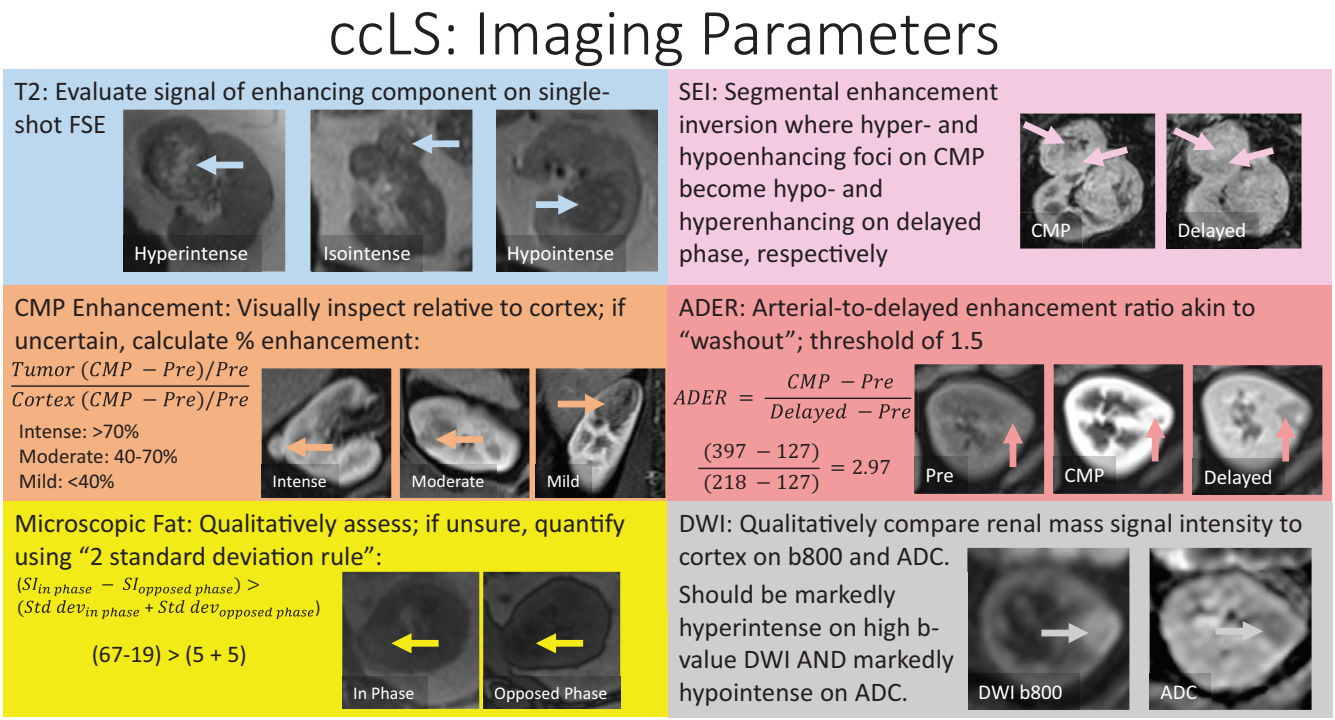

Figure 5. Chart shows the imaging parameters assessed when applying the ccLS algorithm. *ADC* = apparent diffusion coefficient, *b800* = *b* value of 800 sec/mm², *FSE* = fast spin echo.

signal intensity, as the solid component of some renal masses may enhance most conspicuously in a delayed fashion. Subtraction images also aid in detecting enhancement of regions of the mass that may enhance less than normal renal parenchyma and other hyperenhancing foci within the same mass.

T1-weighted Corticomedullary Phase Enhancement.—As the second feature of SRM assessment, enhancement is assessed at the corticomedullary phase (CMP) on T1-weighted gadolinium-enhanced MR images and characterized as intense, moderate, or mild. As with T2-weighted signal intensity, visual assessment of CMP enhancement can be performed initially by comparing the most enhancing portion of the SRM to the normal renal cortex on the same section. If uncertainty persists after visual inspection (particularly in distinguishing moderate from mild enhancement), the percentage of enhancement of the mass from the precontrast phase (*Pre* in the subsequent formula) to the CMP can be compared between the SRM and normal renal cortex by using the following formula:

$$\frac{\text{Tumor (CMP} - \text{Pre)/Pre}}{\text{Cortex (CMP} - \text{Pre)/Pre}}$$

A threshold greater than 75% is used for intense enhancement, between 40% and 75% is used for moderate enhancement, and less than 40% is used for mild enhancement. Using the same sequence type and parameters at each dynamic contrast phase is essential for robust quantification.

Microscopic Fat.—Microscopic fat, the preferred term of the Society of Abdominal Radiology DFP on RCC, refers to a combination of fat and water within a voxel (27) and serves as a major feature in the ccLS algorithm. Microscopic fat can be qualitatively assessed as visually evident signal intensity loss within an SRM when comparing the opposed-phase sequences to the in-phase sequences. Alternatively, hyperintensity identified with a fat-only Dixon sequence that is less than that of adjacent retroperitoneal fat can be considered an indicator of microscopic fat and enables rapid screening of the kidneys for fat-containing lesions, although the presence of microscopic fat should be confirmed on in-phase and opposed-phase images. If uncertainty persists after visual inspection, quantification by using the two standard deviation rule is recommended by comparing the difference of region of interest signal intensities *(SI)* to the sum of standard deviations *(Std dev)* by using the following formula:

$$(\text{SI}_{in\ phase} - \text{SI}_{opposed\ phase}) > (\text{Std dev}_{in\ phase} + \text{Std dev}_{opposed\ phase}).$$

Ancillary Features

Segmental Enhancement Inversion.—Segmental enhancement inversion (SEI) is a dynamic postcontrast imaging finding in which an SRM exhibits differential enhancement in portions of the mass whereby initially hyperenhancing components become hypoenhancing and initially hypoenhancing components become hyperenhancing. This pattern may be attributable to the combination of a compactly arranged cellular component, which initially avidly enhances and subsequently washes out, and a fibrous component, which enhances in a delayed fashion (31). This inversion of enhancement characteristics may be more apparent at delayed phase imaging, such as at 5 minutes, rather than at the nephrographic phase.

A somewhat controversial finding, SEI exhibits poor interobserver agreement in recent studies (20).

Arterial-to-Delayed Enhancement Ratio.—The arterial-to-delayed enhancement ratio (ADER) refers to an SRM exhibiting avid enhancement at CMP imaging and subsequently relative hypoenhancement at delayed phase imaging performed at least 2–3 minutes or later after contrast material administration. Quantitatively, a threshold ratio of greater than or equal to 1.5 is used in the following calculation to be considered positive:

$$\text{ADER} = \frac{\text{CMP} - \text{pre}}{\text{Delayed} - \text{pre}}.$$

If delayed phase imaging is performed in a different plane than the CMP, visual assessment may be substituted for quantification.

Diffusion-weighted Imaging.—In the ccLS algorithm, an SRM is considered to restrict diffusion if the enhancing component exhibits predominantly hyperintense signal intensity on high–*b*-value diffusion-weighted images of at least 800 sec/mm^2, with corresponding hypointensity on the apparent diffusion coefficient (ADC) map.

Homogeneity and Heterogeneity.—Although not formally considered an ancillary feature in the ccLS algorithm, homogeneity of an SRM is used as a tiebreaking feature for T2-hypointense and intensely enhancing masses (6). Homogeneity and heterogeneity are not specifically defined but should be visually assessed with all acquired sequences.

ccLS Algorithm

The ccLS algorithm (Fig 6) establishes a straightforward stepwise approach in applying the observations described previously in assessing renal masses. With the ccLS algorithm, the clinician is provided a Likert score reflecting the likelihood of ccRCC. The score choices include 1 (very unlikely), 2 (unlikely), 3 (intermediate likelihood), 4 (likely), and 5 (very likely). Differential diagnoses (if applicable) that may be considered on the basis of imaging characteristics are also suggested. An online resource is available to work through the algorithm (32). In our experience, calculating the ccLS takes less than 3 minutes for a typical case.

The first step in the ccLS algorithm is establishing whether the algorithm should be used at all. Cystic, nonenhancing, and macroscopic fat-containing masses are excluded from the ccLS. The major criteria of T2-weighted signal intensity (hyperintense, isointense, or hypointense), CMP enhancement (intense, moderate, or mild). and microscopic fat are then assessed in a stepwise fashion. The ancillary features of SEI, ADER, diffusion restriction, and homogeneity need to be assessed, only if directed to do so by the flowchart, in a binary (yes or no) fashion. Tiebreaking rules, presented as footnotes in the ccLS algorithm, are integrated into the provided flowchart for easier use.

After a ccLS is determined, the algorithm also offers other entities to consider in the differential diagnosis on the basis of the combination of imaging features present, such as oncocytoma with SEI, fat-poor AML (fpAML) with an ADER greater than or equal to 1.5 and marked diffusion restriction, pRCC with T2-weighted hypointensity and mild CMP enhancement, and chrRCC based on variable T2-weighted and CMP characteristics. We discuss the various steps to follow in the algorithm by describing the typical imaging features of renal neoplasms and other diagnostically challenging cases.

Typical Imaging Features of Primary SRMs

Clear Cell RCC

The typical ccRCC constitutes one end of the SRM imaging spectrum with T2-weighted isointensity or hyperintensity and intense, often heterogeneous, CMP enhancement (5). To distinguish ccRCC from other T2-hyperintense SRMs such as oncocytomas or chrRCCs, the presence of microscopic fat should be evaluated (Fig 7). Microscopic fat, a consequence of intracytoplasmic lipid and/or glycogen (why the "clear cell" name is used owing to lipid-rich clear cells at histologic examination), is frequently present in the enhancing component of a ccRCC. For non-AML SRMs, microscopic fat is most common in ccRCC but can rarely occur with other histologic conditions (32). Although the ccLS system does not set a specific threshold discriminating ccRCC from other histologic conditions on the basis of the degree of microscopic fat, a 25% signal intensity loss has been proposed elsewhere in the literature (33). DWI characteristics of a ccRCC may overlap with those of benign renal masses, typically with an ADC higher than that of an fpAML or pRCC (33).

Papillary RCC

pRCC constitutes the opposite end of the SRM imaging spectrum when compared with ccRCC. A pRCC typically exhibits T2-weighted hypointensity and mild enhancement in the CMP, with progressive enhancement on delayed phase postcontrast images (Fig 8) (34). A pRCC typically markedly restricts diffusion, a feature that can be helpful in identifying an atypical T2-weighted isointense pRCC. Microscopic fat is not a typical finding of pRCC. pRCCs are more likely than ccRCCs to exhibit intrinsic T1-weighted hyperintensity and magnetic susceptibility related to hemorrhage, but this feature is not currently incorporated into the ccLS (33–39).

Chromophobe RCC

chrRCC does not have a characteristic imaging pattern at MRI, unlike ccRCC and pRCC. A chrRCC can have variable T2-weighted signal intensity (hyperintense or isointense); variable, although frequently homogeneous, CMP enhancement; and well-circumscribed margins (40). The CMP enhancement of a chrRCC can range between that of a pRCC and a ccRCC (Fig 9). Although not integrated into the ccLS algorithm, marked diffusion restriction favors a diagnosis of chrRCC over oncocytoma (41,42).

Oncocytoma

Similar to chrRCCs, oncocytomas can exhibit variable T2-weighted signal intensity (typically hyperintense or isointense) and CMP enhancement (intense or moderate). Diffusion restriction is typically less than that of a chrRCC. An

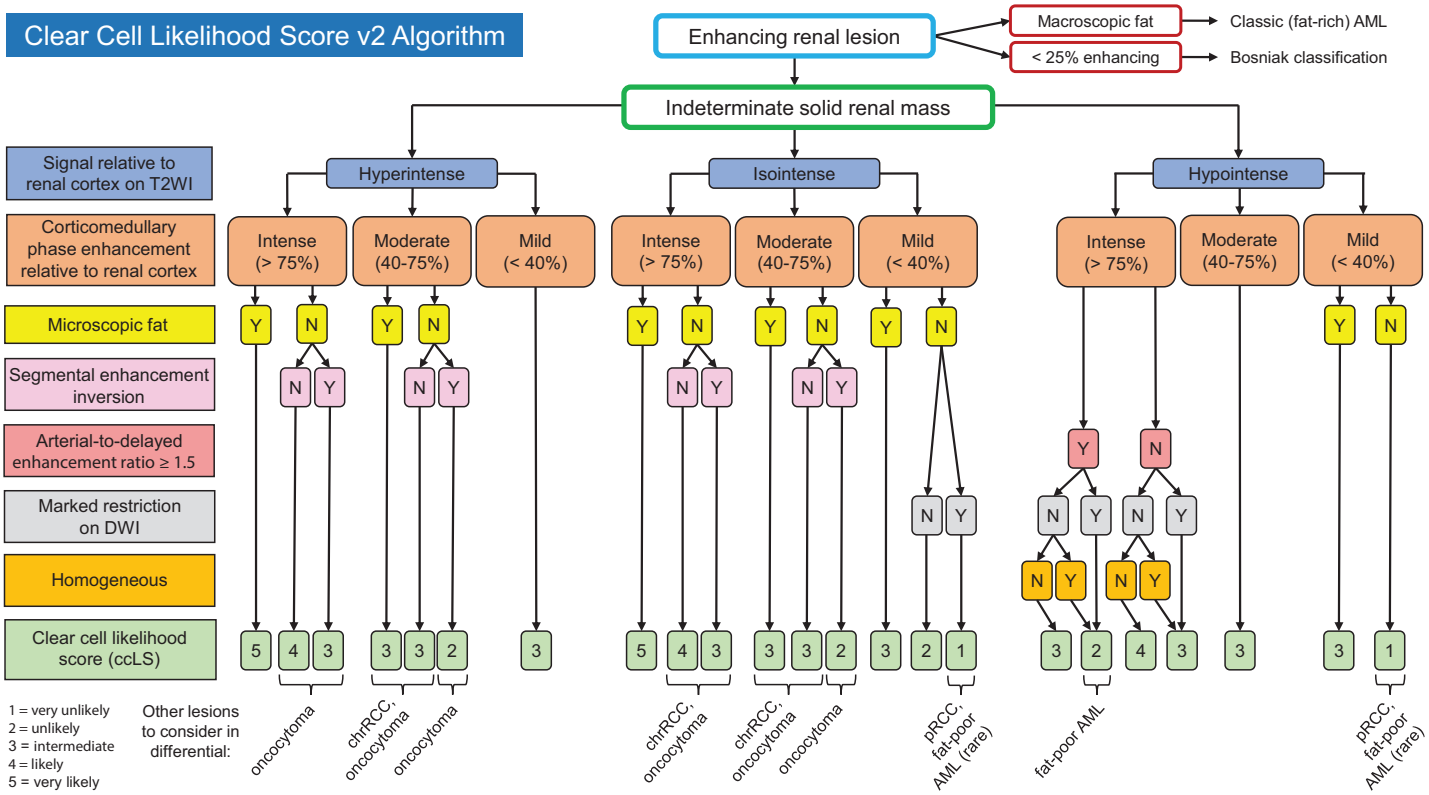

Figure 6. Flowchart shows the ccLS algorithm. An enhancing renal mass (>25% enhancing, nonmacroscopic, and fat containing) should be assessed in a stepwise fashion by first assessing T2-weighted signal intensity and then CMP enhancement (both relative to those of the normal cortex). Additional features such as microscopic fat, SEI, ADER, diffusion restriction, and homogeneity are then applied as needed in the flowchart to determine a ccLS, with scores ranging from 1 (very unlikely) to 5 (very likely) representing the likelihood of ccRCC. The alternative diagnoses to consider on the basis of the imaging features are included below the ccLS. *N* = no, *T2WI* = T2-weighted imaging, *Y* = yes.

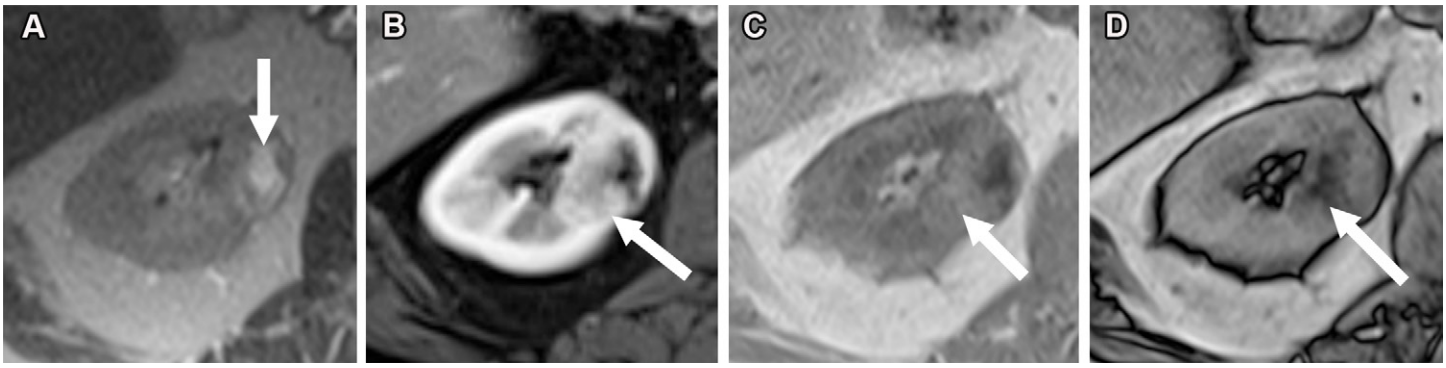

Figure 7. ccRCC in a 65-year-old man. **(A)** Axial T2-weighted MR image shows a heterogeneously T2-hyperintense 3.4-cm right renal mass (arrow). **(B)** Axial postcontrast CMP T1-weighted MR image shows intense enhancement of the solid component of the mass (arrow). **(C, D)** Axial in-phase **(C)** and opposed-phase **(D)** T1-weighted MR images show in-phase hyperintense signal (arrow in **C**), which becomes hypointense (arrow in **D**) and is consistent with the presence of microscopic fat. The ccLS is 5 (very likely ccRCC). A grade 3 ccRCC was found at partial nephrectomy.

imaging feature described with oncocytoma is SEI. However, this feature is controversial since some RCCs may also exhibit SEI (Fig 10) (43). The reported sensitivity and specificity for SEI at MRI were 15% and 90%, respectively (43). Nevertheless, in the ccLS algorithm, this feature triggers the suggestion of oncocytoma as a differential diagnosis.

Fat-poor AML

Unlike their classic (fat-rich) counterparts, fpAMLs typically contain little to no visible macroscopic or microscopic fat. These masses are typically homogeneously T2 hypointense (like pRCCs) but intensely enhancing at CMP imaging (unlike pRCCs) owing to their angiomatous components. Unfortunately, a small minority of atypical ccRCCs can exhibit similar features. Two other imaging features are helpful for suggesting a diagnosis of fpAML: diffusion restriction and elevated ADER (Fig 11) (44). Marked diffusion restriction is a hallmark of fpAML and much less common with ccRCC (45). Although ccRCC and fpAML can both become hypointense at delayed phase imaging, fpAML typically does so to a greater degree. Hence, a threshold ADER greater than or equal to 1.5 suggests a diagnosis of fpAML in this setting

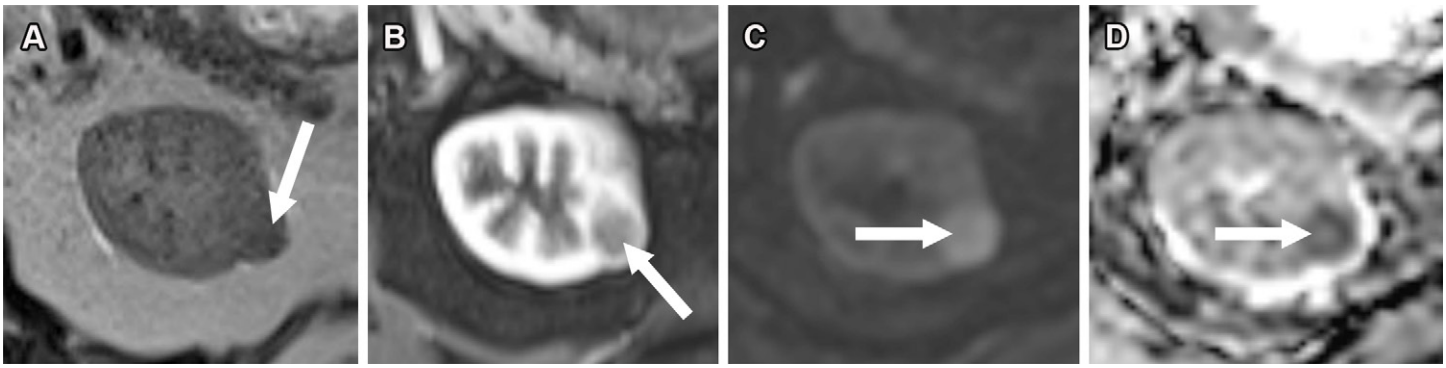

Figure 8. pRCC initially incidentally identified at MRI of the spine in a 67-year-old man. **(A)** Axial T2-weighted MR image shows a T2-hypointense 1.5-cm left renal mass (arrow). **(B)** Axial postcontrast CMP T1-weighted MR image shows mild enhancement of the mass (arrow). **(C, D)** Axial diffusion-weighted MR image (**C**; *b* value = 800 sec/mm^2) shows marked hyperintensity (arrow), and axial ADC map **(D)** shows corresponding hypointensity (arrow). The ccLS is 1 (very unlikely to be ccRCC), with the primary consideration being pRCC, although fpAML can rarely have this appearance.

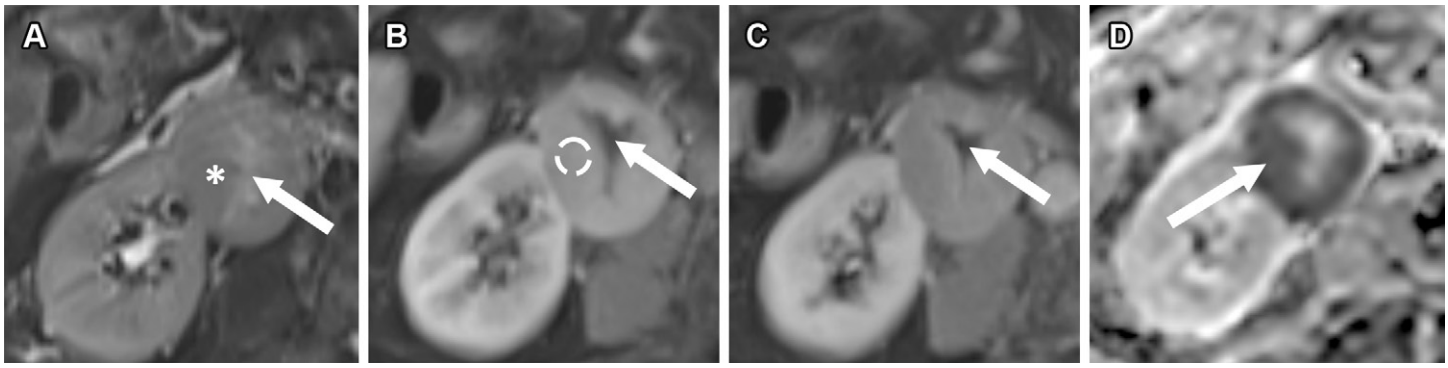

Figure 9. chrCC incidentally found at US in a 78-year-old man with incomplete bladder emptying. **(A)** Axial T2-weighted fat-suppressed MR image shows predominant T2 isointensity (arrow) within a 3.8-cm right renal mass (*). **(B)** Axial postcontrast CMP T1-weighted MR image shows intense enhancement (arrow) of the mass (75% mass-to-cortex ratio), which was measured in the most enhancing portion (dashed circle). **(C)** Axial postcontrast delayed phase T1-weighted MR image shows no segmental enhancement inversion. A nonenhancing central scar (arrow) is present, suggesting oncocytoma as a possible differential diagnosis. **(D)** Axial ADC map shows marked diffusion (arrow) restriction of the mass. The ccLS is 4 (likely ccRCC) with a differential diagnosis of chrRCC, particularly given the marked diffusion restriction. Biopsy revealed a grade 2 chrRCC.

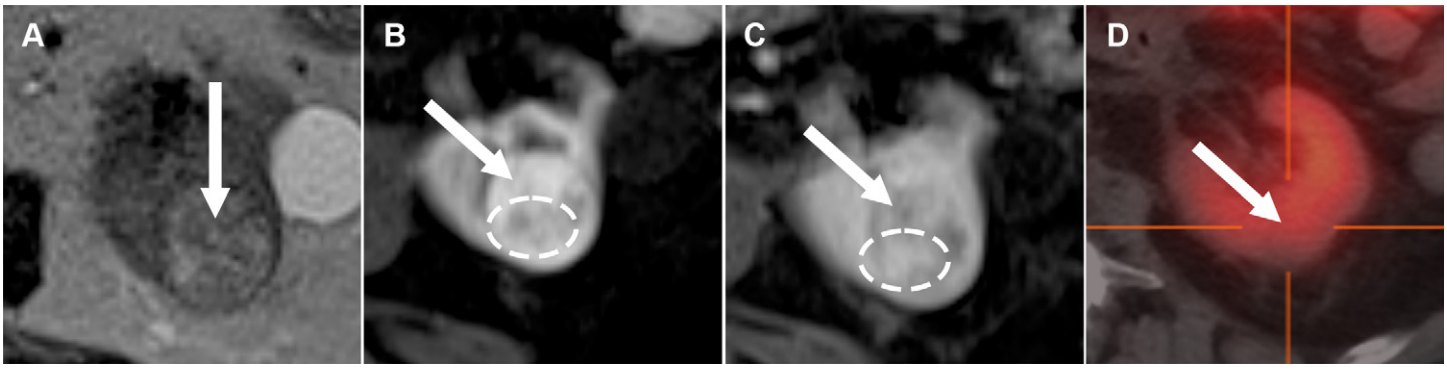

Figure 10. Oncocytoma in a 77-year-old man who previously underwent resection of a left renal oncocytoma. **(A)** Axial T2-weighted MR image shows a T2-hyperintense 2.4-cm left renal mass (arrow). **(B)** Axial postcontrast CMP T1-weighted MR image shows intense enhancement of portions of the mass (arrow), with less enhancement centrally (dashed oval). The most enhancing portion of the mass is used to categorize the degree of enhancement. **(C)** Axial postcontrast delayed phase T1-weighted MR image shows SEI, with hypoenhancement of the initially hyperenhancing components (arrow) and hyperenhancement of the initially hypoenhancing components (dashed oval). No microscopic fat was present (not shown). Given the imaging features and prior history of the patient, a diagnosis of oncocytoma was suggested, with a ccLS of 3 (intermediate likelihood of ccRCC). **(D)** Axial technetium 99m–sestamibi fused SPECT/CT image shows lesional tracer uptake (arrow) similar to that seen in the normal renal parenchyma, suggesting an oncocytic neoplasm. The mass has grown slowly over 6 years of surveillance, doubling in diameter, which suggests indolence.

(46). Homogeneity is used as a tiebreaking rule in downgrading the ccLS of a T2-hypointense intensely enhancing mass, as an fpAML is more commonly homogeneous than a ccRCC (47).

If macroscopic fat is questionably present in only a small volume, it may be reasonable to apply a ccLS to the other portions of the mass, rather than categorizing an SRM as a classic (fat-rich) AML. In many such cases, other features of fpAML

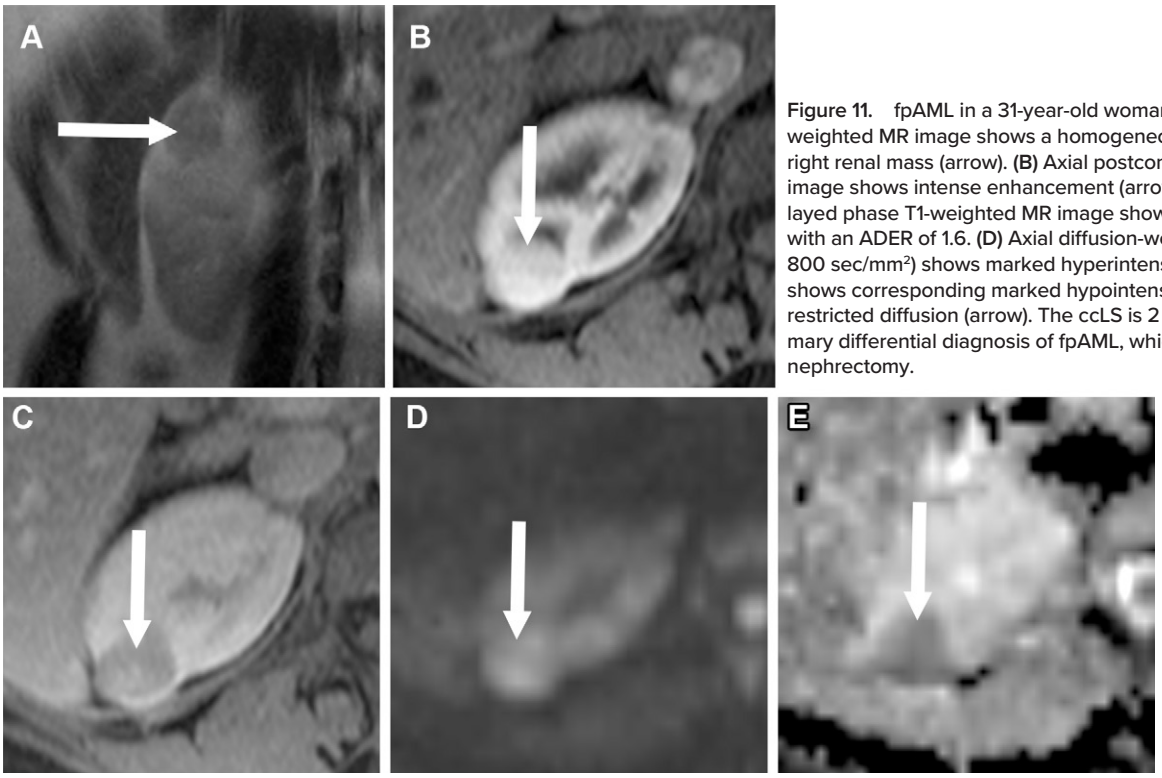

Figure 11. fpAML in a 31-year-old woman with lupus. **(A)** Coronal T2-weighted MR image shows a homogeneously T2-hypointense 2-cm right renal mass (arrow). **(B)** Axial postcontrast CMP T1-weighted MR image shows intense enhancement (arrow). **(C)** Axial postcontrast delayed phase T1-weighted MR image shows hypoenhancement (arrow), with an ADER of 1.6. **(D)** Axial diffusion-weighted MR image (*b* value = 800 sec/mm^2) shows marked hyperintensity (arrow). **(E)** Axial ADC map shows corresponding marked hypointensity, consistent with marked restricted diffusion (arrow). The ccLS is 2 (unlikely ccRCC), with a primary differential diagnosis of fpAML, which was confirmed at partial nephrectomy.

will be present and result in a correspondingly low ccLS. Patient demographics may also be useful to consider, as AMLs have a predilection for middle-aged women (48).

Pitfalls and Observations

Atypical Imaging Features

Many SRMs do not exhibit all of the classic imaging features of a particular renal neoplasm, precluding confident imaging-based diagnosis. In these scenarios, the ccLS algorithm provides valuable guidance in determining the probability of an SRM representing a ccRCC or an alternative diagnosis. For example, SEI is assessed in T2-hyperintense and T2-isointense SRMs exhibiting intense or moderate enhancement that do not contain microscopic fat. The presence of SEI decreases the ccLS and increases the likelihood of the SRM being an oncocytoma, but unfortunately SEI is not sufficiently specific for oncocytoma. Figures 12 and 13 show SRMs and findings of SEI in two patients.

A central scar has been posited as a feature of oncocytoma (50). Although it does not specifically play a role in the ccLS algorithm, this feature is captured indirectly by the presence of SEI. Figure 14 demonstrates a differential diagnosis of RCC and oncocytoma that was proposed in the original report on the basis of the presence of a central scar. If the presence of a central scar is to be considered, careful evaluation of delayed phase enhancement is crucial in distinguishing between SEI (delayed hyperenhancement) and central necrosis (nonenhancement). Central scars may also be present in ccRCCs and should be ignored if the ccLS is 4 or 5, indicating a high likelihood of ccRCC.

DWI has been studied extensively in characterizing SRMs, with a lower ADC reported for RCCs compared with that of benign renal neoplasms (51). Figure 15 provides an example in which the DWI findings are discrepant with the typical imaging features of pRCC. For small renal masses, the anatomic colocalization of acquisitions with different *b* values may be inaccurate owing to differences in breathing patterns, leading to incorrect ADC calculations that may account for the findings in this case. The current iteration of the ccLS also does not leverage DWI in assessing oncocytoma (Fig 5), which may be of benefit as most oncocytomas do not exhibit marked diffusion restriction (34).

ccRCCs are not classically T2 hypointense. However, within the ccLS algorithm, there exists a pathway for a heterogeneous T2-hypointense SRM to be likely ccRCC (ccLS 4). This occurs if the mass is heterogeneous, T2 hypointense, and intensely enhancing without ancillary features such as an ADER greater than or equal to 1.5 or marked diffusion restriction that might decrease the ccLS. Figure 16 shows a ccRCC that nearly follows this pathway (except that the mass is homogeneous, which resulted in a ccLS of 3).

fpAMLs typically exhibit intense enhancement at CMP imaging and washout at delayed phase imaging with no visible fat. However, atypical fpAMLs may enhance only mildly and/or contain microscopic fat (35). That said, microscopic fat is far more common in ccRCCs than in fpAMLs (50). Diffusion restriction is not used by the current ccLS algorithm in this setting but may also lead to a diagnosis of fpAML rather than ccRCC. Morphology may offer additional clues, such as the "ice cream cone" pattern that has been described for AMLs in which the SRM has an angular or pyramidal interface with the periphery of the kidney (52). Figure 17 depicts such a case, in which 6 years of stability confirmed the high likelihood of benignity of an SRM that was never sampled.

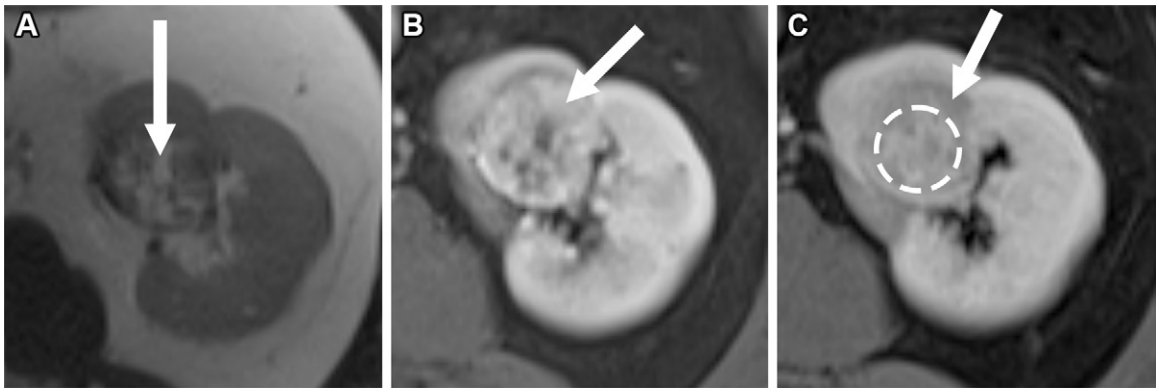

Figure 12. Probable oncocytoma incidentally identified at imaging in a 70-year-old man with shortness of breath. **(A)** Axial T2-weighted MR image shows a T2-hyperintense 3.7-cm left renal mass (arrow). **(B)** Axial postcontrast CMP T1-weighted MR image shows intense enhancement (arrow). **(C)** Axial postcontrast delayed phase T1-weighted MR image shows SEI, in which the hypoenhancing central portion of the mass is now hyperenhancing (dashed circle) relative to the peripheral component (arrow), which was previously hyperenhancing during the CMP. No microscopic fat was present (not shown). The ccLS is 3 (intermediate likelihood of ccRCC), with a differential diagnosis of oncocytoma based on the presence of SEI. On the basis of the patient's age, comorbidities, and probable need for radical rather than partial nephrectomy, the patient was actively surveilled with stability of the mass over 18 months of follow-up.

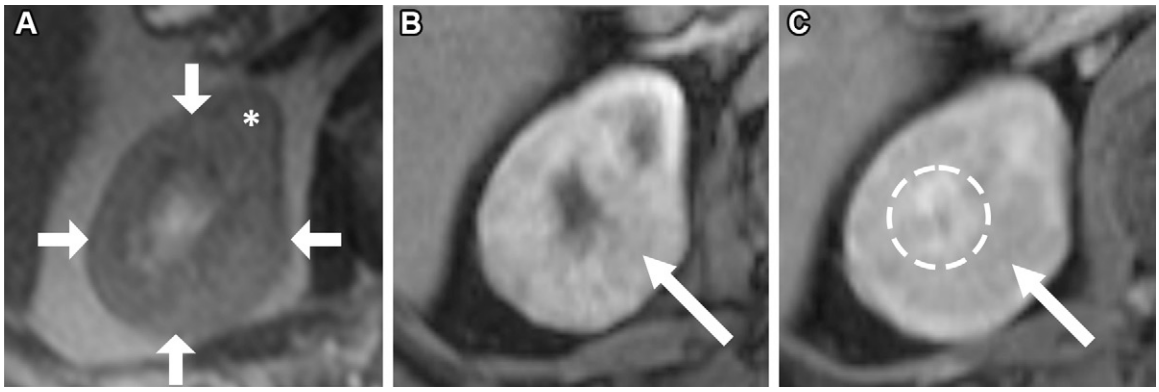

Figure 13. ccRCC in a 57-year-old woman. **(A)** Axial T2-weighted MR image shows a 4.5-cm endophytic renal mass with predominant T2 isointensity (arrows delineate boundaries of the mass) to normal renal parenchyma anteromedially (*). **(B)** Axial postcontrast CMP T1-weighted MR image shows moderate enhancement (arrow). **(C)** Axial delayed phase T1-weighted MR image shows SEI, in which the hypoenhancing central portion of the mass is now hyperenhancing (dashed circle) relative to the peripheral component (arrow), which was hyperenhancing during the CMP. No microscopic fat was present (not shown). The ccLS is 2 (unlikely ccRCC), with an additional differential diagnosis of oncocytoma given the presence of SEI. After a discussion with the urologist regarding the possibility of benignity but the need for long-term surveillance given the patient's age, the patient ultimately opted for nephrectomy, which revealed grade 3 ccRCC. SEI, although suggestive of oncocytoma, can also be seen with RCC.

Hemorrhage presents both challenges and opportunities when using the ccLS algorithm to characterize an SRM. Only enhancing components of a mass should be used for assessment of T2-weighted signal intensity. Thus, attention must be given at T1-weighted postcontrast imaging to exclude cystic foci that contain blood products before assigning a T2-weighted signal intensity. Although hemorrhage associated with an SRM has been seen more frequently in pRCC than in ccRCC in our institutional experience, prior studies have indicated conflicting results (36–38,44).

Technical Considerations

Subtraction imaging is not formally used in the ccLS scheme in assessing the pattern of CMP enhancement but provides a simpler method of assessing the intensity of enhancement, as precontrast T1-weighted signal intensity is automatically factored into the subtracted sequence signal intensities of the SRM and renal cortex. This eliminates a step in the calculation, presuming there is little to no misregistration between the precontrast and CMP acquisitions (Fig 18). It is critical to assess the degree of enhancement in the most avidly enhancing portion of the mass rather than simply measuring it in the center (53).

The use of single-shot fast spin-echo T2-weighted sequences in the ccLS algorithm is advocated with good reason, as image acquisition is faster and less likely to be degraded by motion artifact than would a multishot acquisition. However, the signal-to-noise ratio is lower owing to the undersampling of the k-space, a relevant issue with low-field-strength MRI systems (such as newer 0.55-T units) (Fig S1). A multishot fast spin-echo sequence should be considered a reasonable alternative for assessment if a non–fat-suppressed single-shot fast spin-echo sequence was not performed, as we often encounter at

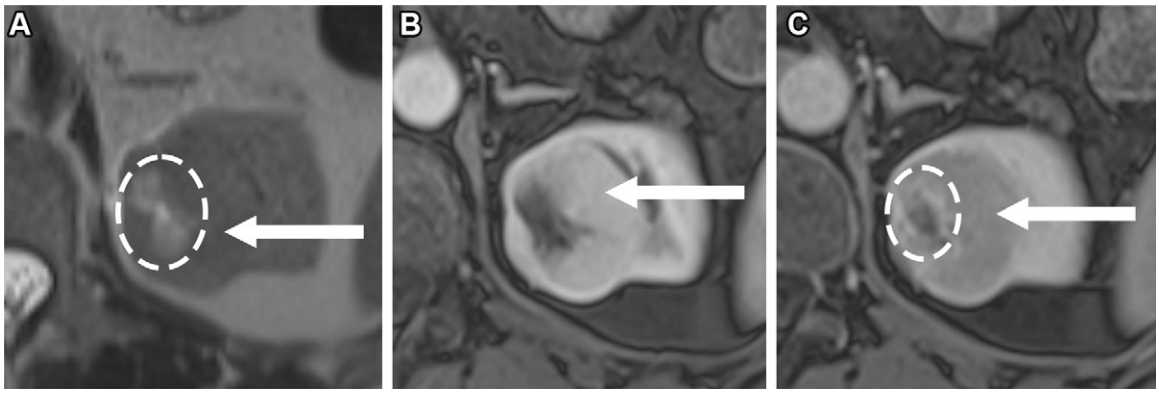

Figure 14. Oncocytoma in a 56-year-old woman with smoldering multiple myeloma incidentally detected at fluorodeoxyglucose PET/CT. **(A)** Axial T2-weighted MR image shows a predominantly T2-isointense 4.4-cm left renal mass (arrow), which is a central T2-hyperintense scar (dashed oval). **(B)** Axial postcontrast delayed phase CMP T1-weighted MR image shows intense enhancement of the periphery of the mass (arrow). **(C)** Axial postcontrast T1-weighted MR image shows SEI, in which the hypoenhancing central portion of the mass is heterogeneously hyperenhancing (dashed oval) relative to the peripheral component (arrow), which was hyperenhancing during the CMP in **B**. The ccLS is 3 (intermediate likelihood of ccRCC), with a differential diagnosis of oncocytoma based on the presence of SEI. Oncocytoma was diagnosed at left partial nephrectomy.

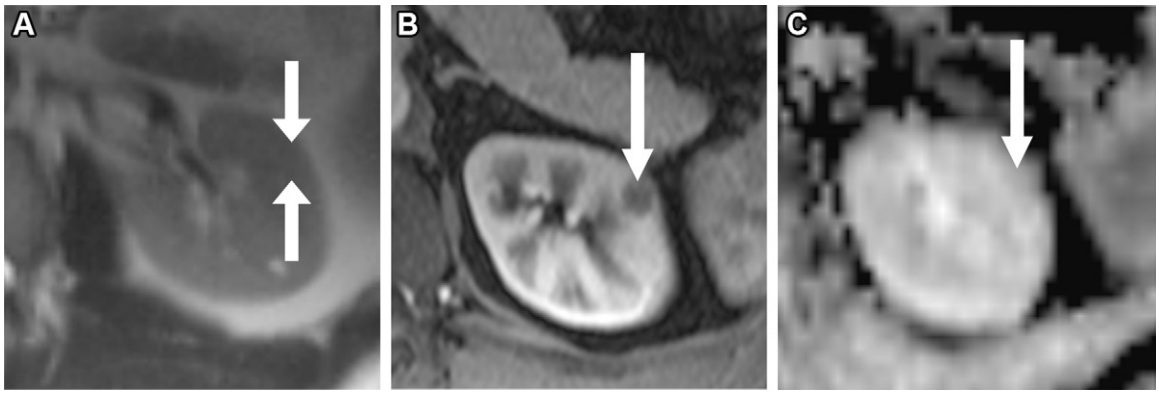

Figure 15. pRCC incidentally detected at abdominal MRI in a 37-year-old man with hepatic steatosis. **(A)** Axial T2-weighted MR image shows a T2-isointense 1.3-cm left renal mass (arrows). **(B)** Axial postcontrast CMP T1-weighted MR image shows mild enhancement (arrow). **(C)** Axial ADC MR image shows no diffusion restriction of the mass (ADC of 2 $\times$ 10^{-3} mm^2/sec) (arrow). The ccLS is 2 (unlikely ccRCC) with a primary consideration of pRCC. Partial nephrectomy revealed a type 2 pRCC with a grade of 3 or 4.

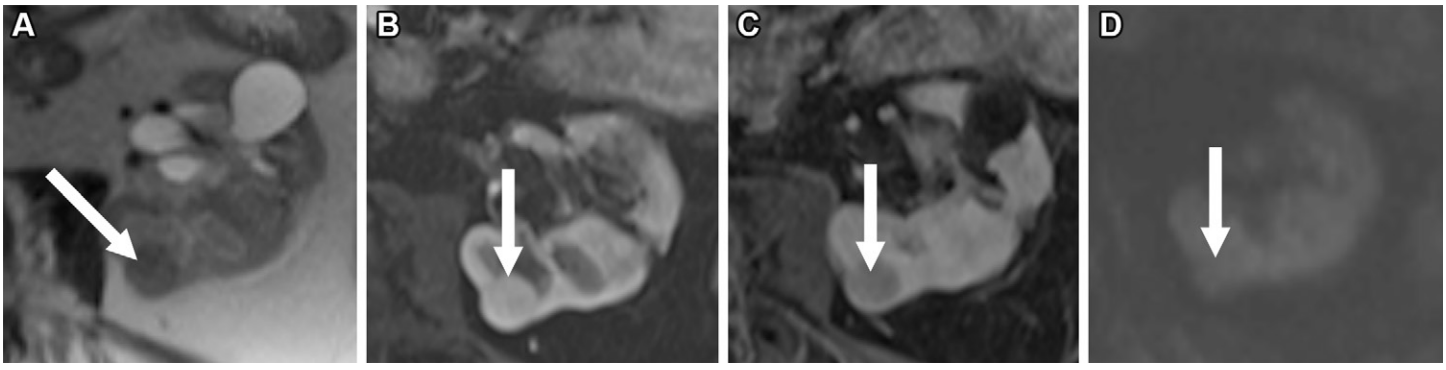

Figure 16. Probable ccRCC incidentally detected at CT colonography in an 82-year-old man. **(A)** Axial T2-weighted MR image shows a homogeneously T2-hypointense 1.9-cm left renal mass (arrow). **(B)** Axial postcontrast CMP T1-weighted MR image shows intense enhancement (arrow). **(C)** Axial delayed phase T1-weighted MR image shows hypointensity of the mass relative to the renal cortex (arrow). The ADER was calculated to be 1.4, which did not reach the threshold of 1.5 to be considered positive. **(D)** Axial diffusion-weighted MR image (*b* value = 800 sec/mm^2) shows no diffusion restriction of the mass (arrow). Microscopic fat was not present (not shown). Homogeneity is the final assessment in the ccLS algorithm for such a mass, with heterogeneity upgrading an SRM to a ccLS of 4 and homogeneity, such as in this mass, resulting in a ccLS of 3 (likely ccRCC). Biopsy was deferred owing to the patient's age and comorbidities, and the mass was actively surveilled for 4 years and grew by about 50% in maximal diameter during that time. The patient died of other causes.

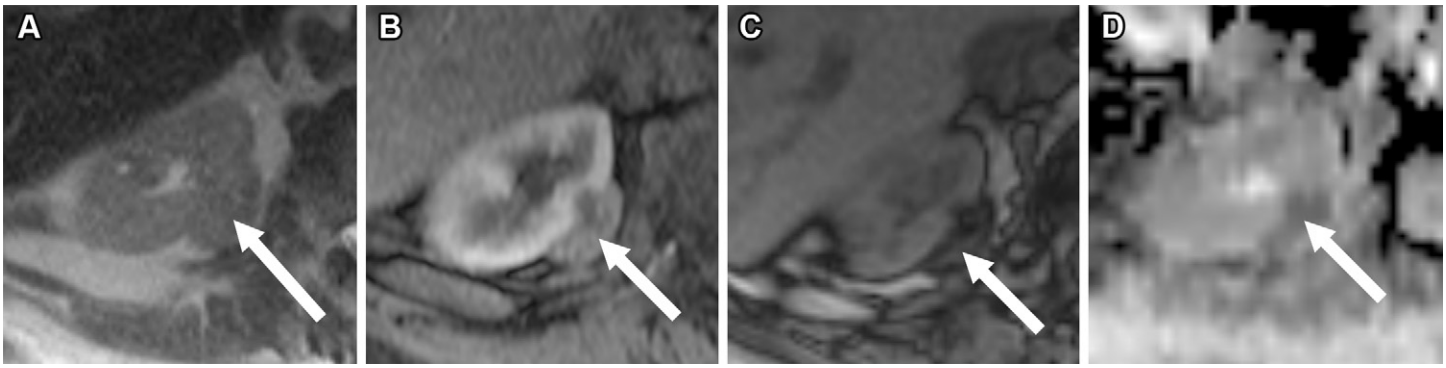

Figure 17. Indolent renal mass incidentally found at CT of the chest in a 72-year-old woman with dyspnea. **(A)** Axial T2-weighted MR image shows a T2-hypointense 2.6-cm right renal mass (arrow). **(B)** Axial postcontrast CMP T1-weighted MR image shows mild enhancement (arrow), along with the "ice cream cone pattern" with an angular interface at the periphery of the kidney. **(C)** Axial opposed-phase T1-weighted MR image shows hypointensity compared with the signal intensity on the in-phase MR image (not shown), consistent with microscopic fat (arrow). **(D)** Axial ADC MR image shows marked hypointensity of the mass (with corresponding hyperintensity on an diffusion-weighted MR image [not shown; *b* value = 800 sec/mm^2]), indicating diffusion restriction (arrow). The ccLS is 3 (intermediate), with no specific differential diagnosis offered by the ccLS algorithm. A diagnosis of fpAML was proposed at initial imaging, and the mass has been stable for 6 years, indicating probable benignity.

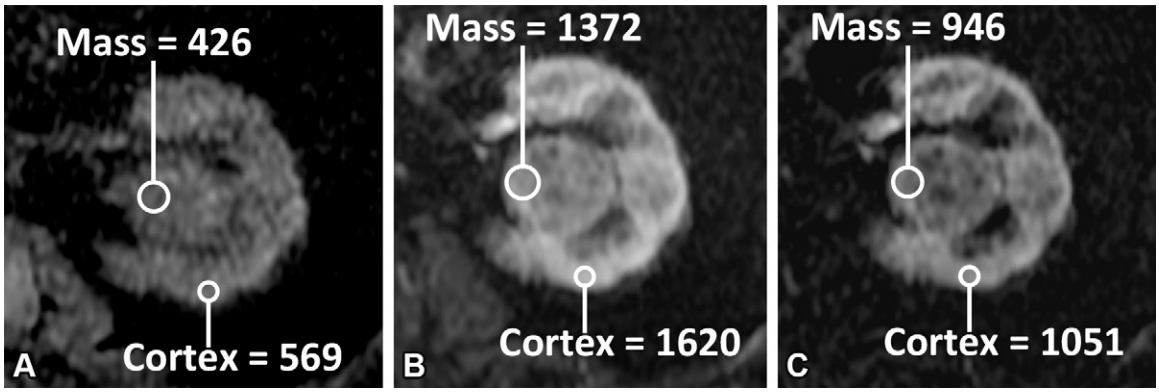

Figure 18. ccRCC in a 63-year-old woman. **(A)** Axial precontrast T1-weighted MR image shows a 3-cm endophytic left renal mass. **(B)** Axial postcontrast CMP T1-weighted MR image shows intense enhancement of the most avidly enhancing portion of the mass (mass signal intensity: 1372 CMP and 426 precontrast; renal cortex signal intensity: 1620 CMP and 569 precontrast; 90% enhancement ratio). **(C)** Axial postcontrast CMP subtraction T1-weighted MR image can be used to simplify the calculation, since the subtraction signal intensity factors in the precontrast signal intensity. The enhancement ratio is (946/426)/(1051/569), or 120%. The mass was T2 hyperintense with microscopic fat (not shown), resulting in a ccLS of 5 (very high likelihood of ccRCC). Left nephrectomy revealed a grade 2 ccRCC.

outside imaging examinations submitted to our institution for rereview. Masses that cannot be assigned a specific score on the basis of their appearance (unusual presentation, poor image quality, etc) should be assigned a ccLS of 3 (intermediate risk).

Other Renal Neoplasms

The current 2022 World Health Organization classification scheme for renal tumors includes over 30 types of renal epithelial neoplasms, which would be impractical to integrate into an imaging system (54). Fortunately, after excluding the five most common diagnoses, the remaining categories collectively represent less than 5% of SRMs. More unusual variants, such as renal medullary carcinoma (an aggressive variant of RCC occurring primarily in patients with the sickle cell trait) (Fig S2), clear cell papillary RCC, and molecularly classified RCCs, are not addressed in the ccLS system. Additionally, in patients with lymphoma (Fig S3), urothelial carcinoma (Fig S4), or nonrenal primary tumors that could metastasize to the kidney (Fig S5), the ccLS may have diminished value (3). In the latter setting, extrarenal disease status (eg, progressive widespread metastatic disease) should be considered when determining the etiologic features of an enlarging renal mass. Rare benign neoplasms, such as neurofibroma (Fig S6) and metanephric adenoma (Fig S7), are not included in the current ccLS algorithm (55).

The ccLS algorithm does not account for patients with a genetic predisposition for developing renal masses, such as in those with tuberous sclerosis (AML), von Hippel–Lindau (ccRCC), Birt-Hogg–Dubé (chrRCC, oncocytoma), or hereditary leiomyomatosis and RCC syndrome (pRCC) (56). In such cases, the pretest probability of a specific renal mass should be considered and used to inform the final impression, rather than ccLS alone. For instance, an atypical fpAML is much more common than a ccRCC in a patient with tuberous sclerosis, and a lesion that has features typically indicating a higher ccLS should still be favored to represent an fpAML. Conversely, in von Hippel–Lindau syndrome, nearly all solid renal lesions represent ccRCCs regardless of their imaging appearance and ccLS.

Future Directions

Imaging Stability

Imaging stability or an indolent growth pattern currently is not considered in the ccLS algorithm. Occasionally, a newly identified renal mass may be present in retrospect during a review of prior examinations. Alternatively, a patient enrolled in active surveillance may undergo serial imaging examinations every 6–12 months to establish stability and/or growth rate. A lesion that is stable or has an indolent pattern of growth could conceivably be downgraded in its ccLS, in a manner similar to that used in the Liver Imaging Reporting and Data System (LI-RADS) algorithm, although no such mechanism exists in the current iteration of the ccLS algorithm. After initial evaluation, MRI may not be repeated for surveillance owing to cost considerations. However, there is a role for serial MRI in several scenarios, such as if the SRM cannot be adequately depicted and followed up with US, if the SRM is occult at single-phase portal venous CT, if the SRM is in a young patient, or if there is clinical desire to minimize potential long-term ionizing radiation exposure from multiphasic CT examinations. Further research may support the application of criteria to downgrade the ccLS on the basis of growth patterns.

Grade and Clinical Management

Clinical management strategies based on the ccLS system have been proposed: SRMs with a ccLS of 4 or 5 are recommended to undergo definitive management, SRMs with a ccLS of 3 are referred for biopsy, and SRMs with a ccLS of 1 or 2 undergo active surveillance when appropriate (6,57). This approach could potentially reduce overtreatment of benign or indolent SRMs. However, a reported 18% of SRMs with a ccLS of 1 or 2 are high-grade neoplasms (International Society of Urological Pathology grade of 3 or 4), and with such an approach, approximately 5% of high-grade neoplasms among SRMs would be recommended for active surveillance. Thus, the low probability of a patient developing metastatic disease while under surveillance needs to be carefully weighed. Furthermore, the ccLS assumes that knowledge of ccRCC would prompt definitive therapy, when in many cases, it would not without knowledge of the grade of the tumor. Noninvasive assessment of tumor grading at imaging by using radiomic features and machine learning remains an ongoing investigation (58), with potential applications to future iterations of the ccLS.

Novel Molecular Tools

Novel molecular tools may further improve the ability of imaging to diagnose and stage ccRCC noninvasively. Technetium 99m–sestamibi SPECT/CT has been studied to distinguish tumors in the oncocytoma-chRCC spectrum from other renal neoplasms by using a cutoff tumor-to-background radiotracer uptake ratio greater than 0.6, with reported specificity of 96%, although the relatively low spatial resolution of SPECT makes it impractical for lesions smaller than 2.0 cm (59). However, reports from other institutions have indicated a lower sensitivity and specificity of 66.7% and 89.5%, respectively (60). How to integrate this information into future iterations of the ccLS algorithm remains to be determined. In a recent phase III clinical trial, the PET agent zirconium-89 girentuximab demonstrated high diagnostic accuracy for the diagnosis of ccRCC in patients with indeterminate renal masses (61). Thus, if it is U.S. Food and Drug Administration approved, this agent could supplement the MRI-based renal mass characterizations afforded by the ccLS algorithm.

CT-based Algorithm for ccLS

MRI offers more comprehensive evaluation of renal masses than multiphasic CT, but CT remains the primary imaging option for many patients owing to the cost, availability, and safety. A nascent CT equivalent of the MRI ccLS has been recently proposed (62). Although it still needs further evaluation before widespread adoption (63), the proposed CT-based algorithm has potential benefits compared to the more complex MRI-based ccLS system. The CT-based algorithm relies on mass-to-cortex corticomedullary enhancement ratios and tumor heterogeneity in assigning a likelihood score of 1–5, with a negative predictive value of a CT score of 2 or less, similar to that of the MRI-based ccLS system. A validated CT companion system for the MRI-based ccLS system, in a similar fashion to liver mass imaging with the LI-RADS, may aid in adoption of standardized imaging evaluation of SRMs.

Conclusion

Renal mass evaluation continues to evolve with increasing use of active surveillance of patients with SRMs. SRMs present a challenge and opportunity for the radiologist to improve the patient outcome via more accurate initial management, as active surveillance may be the best initial option for patients with indolent renal neoplasms. Optimal evaluation of the SRM at MRI requires a nuanced approach, integrating multiple parameters when forming an ordered differential diagnosis. In this article, we review the key concepts when applying the ccLS system to characterize SRMs. By describing the application of the ccLS system, we aim to empower the radiologist to characterize SRMs in a more accurate and clinically useful fashion, thereby providing the urologist and patient with improved tools to optimize shared decision making for initial management.

Author affiliations.—From the Mallinckrodt Institute of Radiology (A.S.S., T.J.F., D.H.B., M.J.H., M.I., M.Z.R., M.H.L., B.M.C., A.L.M., J.A.C.L., J.C., C.R.C., R.S.H., M.M., J.G.U., C.L.S., D.R.L.) and Division of Urologic Surgery (E.H.K.), Washington University School of Medicine, 510 S Kingshighway Blvd, Campus Box 8131, St Louis, MO 63110. Presented as an education exhibit at the 2022 RSNA Annual Meeting. Received December 5, 2022; revision requested January 10, 2023, and received January 23; accepted January 26. **Address correspondence to** A.S.S. (email: *anup.shetty@wustl.edu*).

Disclosures of conflicts of interest.—**T.J.F.** Research grant from Siemens AG, consulting fees from Arterys, payment for honoraria from PrecisCa Oncology, payment for expert witness testimony from the State of Florida Ross Feller Casey LLP. **M.I.** Grant from American College of Radiology. All other authors, the editor, and the reviewers have disclosed no relevant relationships.

References

1. Capitanio U, Bensalah K, Bex A, et al. Epidemiology of Renal Cell Carcinoma. Eur Urol 2019;75(1):74–84.

2. Roussel E, Capitanio U, Kutikov A, et al. Novel Imaging Methods for Renal Mass Characterization: A Collaborative Review. Eur Urol 2022;81(5):476–488.
3. Kay FU, Pedrosa I. Imaging of Solid Renal Masses. Radiol Clin North Am 2017;55(2):243–258.
4. Kay FU, Pedrosa I. Imaging of Solid Renal Masses. Urol Clin North Am 2018;45(3):311–330.
5. Diaz de Leon A, Davenport MS, Silverman SG, Schieda N, Cadeddu JA, Pedrosa I. Role of Virtual Biopsy in the Management of Renal Masses. AJR Am J Roentgenol 2019;212(6):1234–1243.
6. Pedrosa I, Cadeddu JA. How We Do It: Managing the Indeterminate Renal Mass with the MRI Clear Cell Likelihood Score. Radiology 2022;302(2):256–269.
7. O'Connor SD, Pickhardt PJ, Kim DH, Oliva MR, Silverman SG. Incidental finding of renal masses at unenhanced CT: prevalence and analysis of features for guiding management. AJR Am J Roentgenol 2011;197(1):139–145.
8. Herts BR, Silverman SG, Hindman NM, et al. Management of the Incidental Renal Mass on CT: A White Paper of the ACR Incidental Findings Committee. J Am Coll Radiol 2018;15(2):264–273.
9. Silverman SG, Israel GM, Herts BR, Richie JP. Management of the Incidental Renal Mass. Radiology 2008;249(1):16–31.
10. Johnson DC, Vukina J, Smith AB, et al. Preoperatively misclassified, surgically removed benign renal masses: a systematic review of surgical series and United States population level burden estimate. J Urol 2015;193(1):30–35.
11. Lee H, Lee JK, Kim K, et al. Risk of metastasis for T1a renal cell carcinoma. World J Urol 2016;34(4):553–559.
12. Kapur P, Zhong H, Araj E, et al. Predicting Oncologic Outcomes in Small Renal Tumors. Eur Urol Oncol 2022;5(6):687–694.
13. Volpe A, Cadeddu JA, Cestari A, et al. Contemporary management of small renal masses. Eur Urol 2011;60(3):501–515.
14. Schieda N, Krishna S, Pedrosa I, Kaffenberger SD, Davenport MS, Silverman SG. Active Surveillance of Renal Masses: The Role of Radiology. Radiology 2022;302(1):11–24.
15. Finelli A, Cheung DC, Al-Matar A, et al. Small Renal Mass Surveillance: Histology-specific Growth Rates in a Biopsy-characterized Cohort. Eur Urol 2020;78(3):460–467.
16. Marconi L, Dabestani S, Lam TB, et al. Systematic Review and Meta-analysis of Diagnostic Accuracy of Percutaneous Renal Tumour Biopsy. Eur Urol 2016;69(4):660–673.
17. Posielski NM, Bui A, Wells SA, et al. Risk Factors for Complications and Nondiagnostic Results following 1,155 Consecutive Percutaneous Core Renal Mass Biopsies. J Urol 2019;201(6):1080–1087.
18. Canvasser NE, Kay FU, Xi Y, et al. Diagnostic Accuracy of Multiparametric Magnetic Resonance Imaging to Identify Clear Cell Renal Cell Carcinoma in cT1a Renal Masses. J Urol 2017;198(4):780–786.
19. Schieda N, Davenport MS, Silverman SG, et al. Multicenter Evaluation of Multiparametric MRI Clear Cell Likelihood Scores in Solid Indeterminate Small Renal Masses. Radiology 2022;303(3):590–599.
20. Dunn M, Linehan V, Clarke SE, Keough V, Nelson R, Costa AF. Diagnostic Performance and Interreader Agreement of the MRI Clear Cell Likelihood Score for Characterization of cT1a and cT1b Solid Renal Masses: An External Validation Study. AJR Am J Roentgenol 2022;219(5):793–803.
21. Steinberg RL, Rasmussen RG, Johnson BA, et al. Prospective performance of clear cell likelihood scores (ccLS) in renal masses evaluated with multiparametric magnetic resonance imaging. Eur Radiol 2021;31(1):314–324.
22. Rasmussen RG, Xi Y, Sibley RC 3rd, Lee CJ, Cadeddu JA, Pedrosa I. Association of Clear Cell Likelihood Score on MRI and Growth Kinetics of Small Solid Renal Masses on Active Surveillance. AJR Am J Roentgenol 2022;218(1):101–110.
23. Campbell SC, Clark PE, Chang SS, Karam JA, Souter L, Uzzo RG. Renal Mass and Localized Renal Cancer: Evaluation, Management, and Follow-Up: AUA Guideline—Part I. J Urol 2021;206(2):199–208.
24. Silverman SG, Pedrosa I, Ellis JH, et al. Bosniak Classification of Cystic Renal Masses, Version 2019: An Update Proposal and Needs Assessment. Radiology 2019;292(2):475–488.
25. Schieda N, Davenport MS, Krishna S, et al. Bosniak Classification of Cystic Renal Masses, Version 2019: A Pictorial Guide to Clinical Use. RadioGraphics 2021;41(3):814–828.
26. Edney E, Davenport MS, Curci N, et al. Bosniak classification of cystic renal masses, version 2019: interpretation pitfalls and recommendations to avoid misclassification. Abdom Radiol (NY) 2021;46(6):2699–2711.
27. Schieda N, Davenport MS, Pedrosa I, et al. Renal and adrenal masses containing fat at MRI: Proposed nomenclature by the society of abdominal radiology disease-focused panel on renal cell carcinoma. J Magn Reson Imaging 2019;49(4):917–926.
28. Salari R, Ballard DH, Hoegger MJ, Young D, Shetty AS. Fat-only Dixon: how to use it in body MRI. Abdom Radiol (NY) 2022;47(7):2527–2544.
29. Wang ZJ, Davenport MS, Silverman SG, et al. MRI renal mass protocol v1.0. Society of Abdominal Radiology Disease Focused Panel on Renal Cell Carcinoma. https://abdominalradiology.org/wp-content/uploads/2020/11/RCC.MRIprotocolfinal-7-15-17.pdf. Accessed November 30, 2022.
30. Alfaleh H, Melkus G, Nasiyabi KA, McInnes MDF, Schieda N. Comparison of image quality and depiction of microscopic fat at 2-D and 3-D T1-weighted (T1W) chemical shift (dual-echo) MRI for evaluation of adrenal adenomas. Abdom Radiol (NY) 2022;47(11):3828–3837.
31. Woo S, Cho JY, Kim SH, et al. Segmental enhancement inversion of small renal oncocytoma: differences in prevalence according to tumor size. AJR Am J Roentgenol 2013;200(5):1054–1059.
32. ccLS Calculator. https://cclsrads.com/. Accessed January 12, 2023.
33. Karlo CA, Donati OF, Burger IA, et al. MR imaging of renal cortical tumours: qualitative and quantitative chemical shift imaging parameters. Eur Radiol 2013;23(6):1738–1744.
34. Kang SK, Zhang A, Pandharipande PV, Chandarana H, Braithwaite RS, Littenberg B. DWI for Renal Mass Characterization: Systematic Review and Meta-Analysis of Diagnostic Test Performance. AJR Am J Roentgenol 2015;205(2):317–324.
35. de Silva S, Lockhart KR, Aslan P, et al. Differentiation of renal masses with multi-parametric MRI: the de Silva St George classification scheme. BMC Urol 2022;22(1):141.
36. Kim C-W, Shanbhogue KP, Schreiber-Zinaman J, Deng FM, Rosenkrantz AB. Visual Assessment of the Intensity and Pattern of T1 Hyperintensity on MRI to Differentiate Hemorrhagic Renal Cysts From Renal Cell Carcinoma. AJR Am J Roentgenol 2017;208(2):337–342.
37. Oliva MR, Glickman JN, Zou KH, et al. Renal cell carcinoma: t1 and t2 signal intensity characteristics of papillary and clear cell types correlated with pathology. AJR Am J Roentgenol 2009;192(6):1524–1530.
38. Kim S, Jain M, Harris AB, et al. T1 hyperintense renal lesions: characterization with diffusion-weighted MR imaging versus contrast-enhanced MR imaging. Radiology 2009;251(3):796–807.
39. Childs DD, Clingan MJ, Zagoria RJ, et al. In-phase signal intensity loss in solid renal masses on dual-echo gradient-echo MRI: association with malignancy and pathologic classification. AJR Am J Roentgenol 2014;203(4):W421–W428.
40. Marko J, Craig R, Nguyen A, Udager AM, Wolfman DJ. Chromophobe Renal Cell Carcinoma with Radiologic-Pathologic Correlation. RadioGraphics 2021;41(5):1408–1419.
41. Metin M, Aydın H, Karaoğlanoğlu M. Renal Cell Carcinoma or Oncocytoma? The Contribution of Diffusion-Weighted Magnetic Resonance Imaging to the Differential Diagnosis of Renal Masses. Medicina (Kaunas) 2022;58(2):221.
42. Zhong Y, Wang H, Shen Y, et al. Diffusion-weighted imaging versus contrast-enhanced MR imaging for the differentiation of renal oncocytomas and chromophobe renal cell carcinomas. Eur Radiol 2017;27(12):4913–4922.
43. Schieda N, Al-Subhi M, Flood TA, El-Khodary M, McInnes MD. Diagnostic accuracy of segmental enhancement inversion for the diagnosis of renal oncocytoma using biphasic computed tomography (CT) and multiphase contrast-enhanced magnetic resonance imaging (MRI). Eur Radiol 2014;24(11):2787–2794.
44. Wilson MP, Patel D, Katlariwala P, Low G. A review of clinical and MR imaging features of renal lipid-poor angiomyolipomas. Abdom Radiol (NY) 2021;46(5):2072–2078.
45. Li H, Li A, Zhu H, et al. Whole-Tumor Quantitative Apparent Diffusion Coefficient Histogram and Texture Analysis to Differentiation of Minimal Fat Angiomyolipoma from Clear Cell Renal Cell Carcinoma. Acad Radiol 2019;26(5):632–639.
46. Sasiwimonphan K, Takahashi N, Leibovich BC, Carter RE, Atwell TD, Kawashima A. Small (<4 cm) renal mass: differentiation of angiomyolipoma without visible fat from renal cell carcinoma utilizing MR imaging. Radiology 2012;263(1):160–168.
47. Lim RS, Flood TA, McInnes MDF, Lavallee LT, Schieda N. Renal angiomyolipoma without visible fat: Can we make the diagnosis using CT and MRI? Eur Radiol 2018;28(2):542–553.
48. Fittschen A, Wendlik I, Oeztuerk S, et al. Prevalence of sporadic renal angiomyolipoma: a retrospective analysis of 61,389 in- and out-patients. Abdom Imaging 2014;39(5):1009–1013.
49. Ishigami K, Jones AR, Dahmoush L, Leite LV, Pakalniskis MG, Barloon TJ. Imaging spectrum of renal oncocytomas: a pictorial review with pathologic correlation. Insights Imaging 2015;6(1):53–64.
50. Lassel EA, Rao R, Schwenke C, Schoenberg SO, Michaely HJ. Diffusion-weighted imaging of focal renal lesions: a meta-analysis. Eur Radiol 2014;24(1):241–249.
51. Hindman N, Ngo L, Genega EM, et al. Angiomyolipoma with minimal fat: can it be differentiated from clear cell renal cell carcinoma by using standard MR techniques? Radiology 2012;265(2):468–477.

52. Kim KH, Yun BH, Jung SI, et al. Usefulness of the ice-cream cone pattern in computed tomography for prediction of angiomyolipoma in patients with a small renal mass. Korean J Urol 2013;54(8):504–509.
53. Sun MRM, Ngo L, Genega EM, et al. Renal cell carcinoma: dynamic contrast-enhanced MR imaging for differentiation of tumor subtypes—correlation with pathologic findings. Radiology 2009;250(3):793–802.
54. Moch H, Amin MB, Berney DM, et al. The 2022 World Health Organization Classification of Tumours of the Urinary System and Male Genital Organs-Part A: Renal, Penile, and Testicular Tumours. Eur Urol 2022;82(5):458–468.
55. Woo S, Cho JY. Imaging findings of common benign renal tumors in the era of small renal masses: differential diagnosis from small renal cell carcinoma—current status and future perspectives. Korean J Radiol 2015;16(1):99–113.
56. Maher ER. Hereditary renal cell carcinoma syndromes: diagnosis, surveillance and management. World J Urol 2018;36(12):1891–1898.
57. Johnson BA, Kim S, Steinberg RL, de Leon AD, Pedrosa I, Cadeddu JA. Diagnostic performance of prospectively assigned clear cell Likelihood scores (ccLS) in small renal masses at multiparametric magnetic resonance imaging. Urol Oncol 2019;37(12):941–946.
58. Purkayastha S, Zhao Y, Wu J, et al. Differentiation of low and high grade renal cell carcinoma on routine MRI with an externally validated automatic machine learning algorithm. Sci Rep 2020;10(1):19503.
59. Wilson MP, Katlariwala P, Murad MH, Abele J, McInnes MDF, Low G. Diagnostic accuracy of 99mTc-sestamibi SPECT/CT for detecting renal oncocytomas and other benign renal lesions: a systematic review and meta-analysis. Abdom Radiol (NY) 2020;45(8):2532–2541.
60. Parihar AS, Mhlanga J, Ronstrom C, et al. Diagnostic Accuracy of 99mTc-Sestamibi SPECT/CT for Characterization of Solid Renal Masses. J Nucl Med 2023;64(1):90–95.
61. Telix International Pty Ltd. 89Zr-TLX250 for PET/CT Imaging of ccRCC-ZIRCON Study (89ZR-TLX250). https://clinicaltrials.gov/ct2/show/NCT03849118. Published February 21, 2019. Updated November 10, 2022. Accessed November 30, 2022.
62. Al Nasibi K, Pickovsky JS, Eldehimi F, et al. Development of a Multiparametric Renal CT Algorithm for Diagnosis of Clear Cell Renal Cell Carcinoma Among Small (≤ 4 cm) Solid Renal Masses. AJR Am J Roentgenol 2022;219(5):814–823.
63. Shetty AS. Editorial Comment: Toward a CT Equivalent of the MRI Clear Cell Likelihood Score. AJR Am J Roentgenol 2022;219(5):824.